ARTICLE

# Shape-Dependent Biomimetic Inhibition of Enzyme by Nanoparticles and Their Antibacterial Activity

**Sang-Ho Cha,[†,‡] Jin Hong,[∥,⊥] Matt McGuffie,[∥,#] Bongjun Yeom,[†,∥,▽] J. Scott VanEpps,[*,∥,#] and Nicholas A. Kotov[*,†,§,∥,○]**

[†]Department of Chemical Engineering, University of Michigan, Ann Arbor, Michigan 48109, United States, [‡]Department of Chemical Engineering, Kyonggi University, Suwon 443-760, South Korea, [§]Department of Biomedical Engineering, University of Michigan, Ann Arbor, Michigan 48109, United States, [∥]Biointerfaces Institute, University of Michigan, Ann Arbor, Michigan48109, United States, [⊥]China Pharmaceutical University, 24 Tongjiaxiang, Nanjing, Jiangsu Province 210009, China, [#]Department of Emergency Medicine, University of Michigan, Ann Arbor, Michigan 48109, United States, [▽]Department of Chemical Engineering, Myongji University, Yongin 449-728, South Korea, and [○]Department of Materials Science and Engineering, University of Michigan, Ann Arbor, Michigan 48198, United States

**ABSTRACT** Enzyme inhibitors are ubiquitous in all living systems, and their biological inhibitory activity is strongly dependent on their molecular shape. Here, we show that small zinc oxide nanoparticles (ZnO NPs)—pyramids, plates, and spheres—possess the ability to inhibit activity of a typical enzyme $\beta$-galactosidase (GAL) in a biomimetic fashion. Enzyme inhibition by ZnO NPs is reversible and follows classical Michaelis—Menten kinetics with parameters strongly dependent on their geometry. Diverse spectroscopic, biochemical, and computational experimental data indicate that association of GAL with specific ZnO NP geometries interferes with conformational reorganization of the enzyme necessary for its catalytic activity. The strongest inhibition was observed for ZnO nanopyramids and compares favorably to that of the best natural GAL inhibitors while being resistant to proteases. Besides the fundamental significance of this biomimetic function of anisotropic NPs, their capacity to serve as degradation-resistant enzyme inhibitors is technologically attractive and is substantiated by strong shape-specific antibacterial activity against methicillin-resistant *Staphylococcus aureus* (MRSA), endemic for most hospitals in the world.

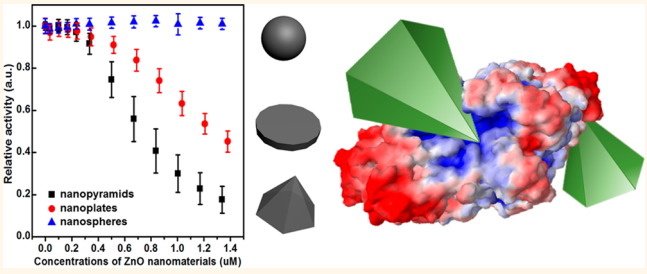


**KEYWORDS:** nanoparticles · enzymes · inhibitors · reaction kinetics · zinc oxide · ZnO · bacteria · MRSA

Enzyme inhibitors are as omnipresent in living organisms as enzymes. They are relevant to a wide spectrum of clinical and technological problems: from antibacterial drugs; to treatment of diabetes,[1] Alzheimes disease,[2] and some cancers;[3] to production of foods,[4] biofuels,[5] and biosensors.[6] Correspondingly, there has been considerable effort to obtain comprehensive understanding of enzyme inhibition over many years. Most studies were focused on the formation of intermolecular lock-and-key complexes with small molecules[7] or complementary proteins and peptides.[8] However, as they are organic in nature, these traditional enzyme inhibitors are unstable and, in turn, are degraded by other enzymes, for instance proteases.

Given the diversity of roles that enzyme inhibitors play, it is imperative to develop new types of inhibitors with unconventional structures that circumvent degradation processes and/or generate different inhibitory effects. Some inorganic nanoparticles (NPs) have been shown to reduce enzyme activity, although the data for NP modulation of enzyme activity are both limited and controversial. Specifically, Vertegel *et al.* reported that adsorption of enzyme onto the surface of spherical NPs with diameters ranging from 4 to 100 nm results in loss of activity.[9] The inhibition effects were attributed to van der Waals (vdW) forces causing irreversible denaturation of the protein.[10] On the basis of these data, NPs can potentially be viewed as nonspecific irreversible inhibitors whose activity correlates with nonspecific binding between enzyme and NP.[11] At the same time, Chalkias *et al.* and Pandey *et al.* reported opposite effects, demonstrating increase in enzyme activity in the presence of NPs.[12,15] In this case,

* Address correspondence to jvane@med.umich.edu, kotov@umich.edu.

Received for review May 29, 2015 and accepted July 29, 2015.

**Published online September 01, 2015**
**10.1021/acsnano.5b03247**

magnetic NPs noticeably increase catalytic activity of horseradish peroxidase. In addition, strong activation of peroxidase activity by cytochrome C was found when this protein adsorbed to 4−35 nm silica NPs.[13] Both activation and deactivation of enzyme were observed with spherical NPs of 11, 50, and 150 nm by Wang *et al.*[14]

Nanoscale dimensions and surface chemistries of NPs coated with organic surface moieties are similar to those of many protein enzyme inhibitors.[16] One can hypothesize that NPs can potentially provide a biomimetic platform to control the catalytic activity of enzymes by replicating the noncovalent interactions between enzymes and traditional biological inhibitors.[16] Improved specificity of inhibition could be achieved by controlling the shape as well as the surface chemistry of NPs. Shape effects would be essential to demonstrate since a large variety of NPs with very diverse geometries can now be prepared. Reversibility of NP−enzyme binding could also be realized *via* better control of electrostatic[17] and vdW forces.[31] Our findings in this study indicate that NP inhibition of biocatalytic processes strongly depends on their shape varying from very weak to exceptionally strong inhibition without denaturation of the enzyme. Analysis of the enzyme inhibition kinetics using Michaelis−Menten formalism reveals inhibitor properties and mechanism not previously seen for other inorganic NPs. Rather, they mimic the properties and mechanism of traditional small molecule-, DNA-, and protein-based inhibitors. Furthermore, the strong shape-dependent inhibitory activity was also observed for planktonic growth of methicillin-resistant *Staphylococcus aureus* (MRSA).

## RESULTS AND DISCUSSION

Looking at potential model systems for this study, we wanted NP inhibitors to be variable in shape, biocompatible and desirably inexpensive. We also wanted the NPs to be small in size and made from light elements in order to reduce vdW forces. Balancing nonspecific vdW attraction with other interactions is necessary in order to minimize denaturation of proteins on the NP surface and NP agglomeration in dispersion. Both factors impede the accuracy of the kinetics analysis, mechanism of inhibitory activity, and the practicality of such inhibitors. Therefore, we chose zinc oxide (ZnO) NPs less than 20 nm in diameter and investigated their effect on the activity of $\beta$-galactosidase (GAL), whose structure and enzymatic activity have been extensively characterized.[18] GAL is a representative carbohydrate energy metabolism enzyme in biological systems and hydrolyses $\beta$-galactosides into monosaccharides. Comparison with the previous case of inhibition of GAL by gold NPs was also essential.[19]

The shape of ZnO NPs was varied to obtain hexagonal nanopyramids,[20] nanoplates, and nanospheres. They were prepared using similar reactions without stabilizers to minimize the effect of the different surface chemistry and distribution of stabilizers on the intermolecular interactions with enzymes. The edges of the hexagonal base of nanopyramids were 15 nm, while their side edges were 18 nm (Figure 1A).[20] The diameter and thickness of nanoplates were 18.4 $\pm$ 2.9 and 3.5 $\pm$ 0.2 nm, respectively (Figure 1B). The diameter of nanospheres was 4.4 $\pm$ 0.5 nm (Figure 1C).

The catalytic activity of GAL was determined by the increase of fluorescence intensity with time due to the accumulation of resorufin which is formed by hydrolysis of resorufin $\beta$-D-galactopyranoside (RGP) *via* GAL. Considering the observations by Wang *et al.*,[14] the smaller ZnO spherical particles might be expected to have the strongest inhibition effects. However, experimental findings were contrary to initial expectations. The inhibition increased greatly from nanospheres to nanoplates to nanopyramids (Figure 1D and Supporting Information Figure S1A−C). Continuous decrease of enzyme activity was observed with increasing concentrations of nanopyramids and nanoplates, while the enzyme activity was found to be virtually invariant for all concentrations of nanospheres. For the latter, inhibition of GAL was not observed even when the concentration of nanospheres exceeded 1.2 $\mu$M. For any concentration, nanopyramids show much higher inhibitory effect on GAL than nanoplates. For example, with 0.5 $\mu$M concentration of nanopyramids, the activity of GAL was reduced by ~25% of the original, whereas the similar concentration of nanoplates led to only ~9% enzyme activity loss. When the concentration of nanopyramids increased to ~1.2 $\mu$M, the activity of GAL dropped to ~20% of the original. However, in the case of nanoplates, GAL still retained about 50% activity.

The preliminary explanation for the mechanism of inhibition involved the denaturation of enzymes on NP surface and/or charge effects, as was observed previously by Dordick *et al.*[9,13] and Rotello *et al.*,[17,21] respectively. However, our experimental data witnessed against these mechanisms for the case of GAL and ZnO. Circular dichroism spectra indicate that the conformation of GAL did not change appreciably in the presence of any concentration or shape of ZnO NPs (Figure 2A). Moreover, the inhibition was reversible unlike cases of NP inhibition previously observed.[10] GAL activity was completely restored when NPs were removed by ethylenediaminetetraacetic acid (EDTA) (Supporting Information Figure S2).

Electrostatic attraction is another possible explanation for the inhibition and its dependence on NP shape; this mechanism would follow the model considered for gold NPs coated with monolayers of charge-bearing thiols[21] and imply complete[10] or partial denaturation accompanied by the conformational change.[19] The isoelectric points of GAL and ZnO NPs are pH 4.6[19]

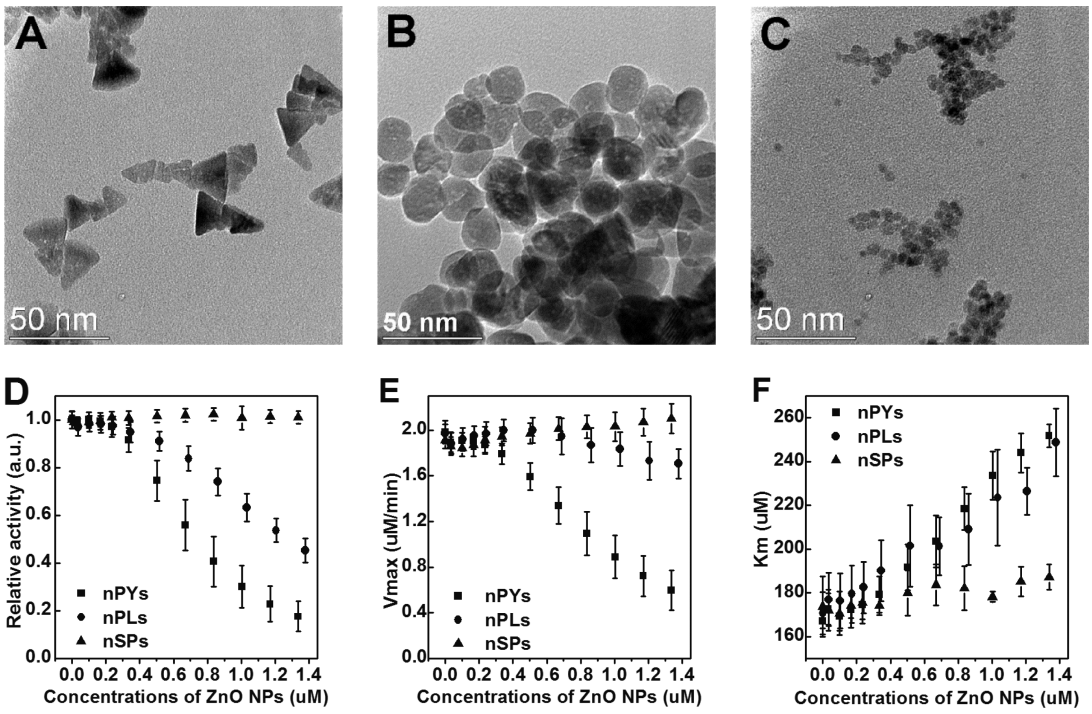


Figure 1. TEM images of ZnO (A) nanopyramids (nPYs), (B) nanoplates (nPLs), and (C) nanospheres (nSPs). (D) Relative catalytic activity of GAL in the presence of three different shaped ZnO NPs after 60 min incubation time. Each relative catalytic activity of GAL with ZnO NPs was normalized with respect to free enzyme activity. The initial concentration of GAL was 0.4 nM. The values for (E) $V_{max}$ and (F) $K_m$ of GAL were calculated from the Michaelis–Menten equation.

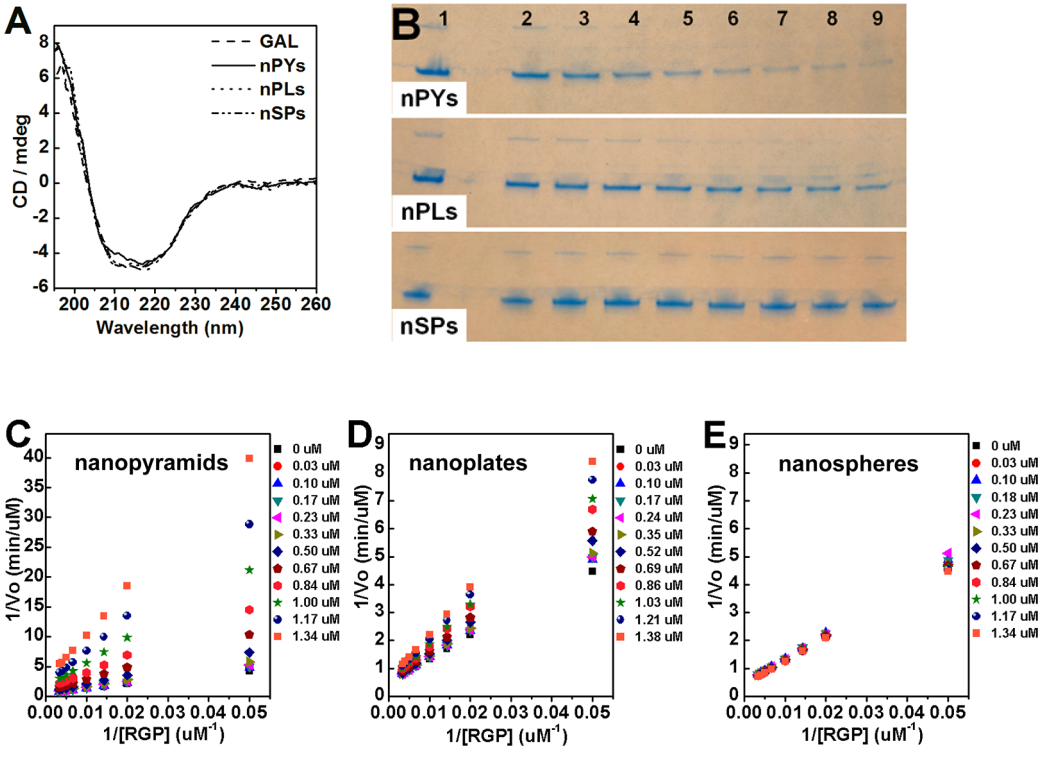


Figure 2. (A) Circular dichroism spectra of GAL in the absence and presence of ZnO NPs. The molar ratio of ZnO NPs to GAL was 0.25. (B) Gel electrophoresis of GAL with various concentrations of ZnO nanopyramids (nPYs), nanoplates (nPLs), and nanospheres (nSPs). The concentrations of ZnO NPs from column 1–9 were 0.00, 0.07, 0.20, 0.34, 0.48, 0.62, 0.75, 0.88, and 1.02 $\mu$M, respectively. The concentration of GAL is 360 nM. (C–E) Lineweaver–Burk plots of the GAL with the various concentrations of ZnO (C) nanopyramids, (D) nanoplates, and (E) nanospheres.

and pH 9,[22] respectively. For intermediate pH 7.5, they are oppositely charged. The electrokinetic zeta potential, $\zeta$, is almost identical for all ZnO NPs used here (Supporting Information Table S1), and therefore, the electrostatic attraction between GAL and ZnO NPs is expected to be nearly the same regardless of shape. This indicates that the inhibition mechanism observed between ZnO and GAL is different from what was observed before with gold[21] or silica NPs[9] of different sizes.[14]

Inability of the previous models to adequately explain the trends of GAL inhibition by ZnO of different shapes prompted us to evaluate the inhibition mechanism of ZnO NPs in greater detail. Following the classical Michaelis–Menten theory of enzyme kinetics, a typical enzyme reaction is described as

$$\mathbf{E} + \mathbf{S} \underset{k_{-1}}{\overset{k_1}{\rightleftarrows}} [\mathbf{ES}] \underset{k_{-2}}{\overset{k_2}{\rightleftarrows}} \mathbf{E} + \mathbf{P} \qquad (1)$$

For the hydrolysis reaction in this study, the substrate (**S**) is nonfluorescent RGP. GAL enzyme (**E**) hydrolyzes RGP *via* an intermediate enzyme–substrate complex (**ES**) then dissociates releasing the fluorescent product resorufin (**P**). Taking advantage of its strong fluorescence, the kinetics of product accumulation was investigated for various concentrations of **S**, **E**, and ZnO NPs. The four rate constants in eq 1 ($k_1$, $k_2$, $k_{-1}$, and $k_{-2}$) were determined (see Supporting Information) and found to be independent of the concentrations and shapes of ZnO NP as well as concentrations of **S** and **E** (Supporting Information Table S2). This point is significant because it further affirms the conclusion that primary, secondary, and tertiary structure of GAL is intact. If the chemical structure or conformation were not retained when ZnO interacts with GAL, there should have been marked changes in some or all kinetic constants. Therefore, the possibility that ZnO NPs might induce "mutation" of the enzyme by substituting one of the catalytic nucleophiles involved in the binding of substrate can be excluded.[23]

Now one can see that ZnO NPs are acting with respect to GAL largely as traditional inhibitors. Hence, the NP induced inhibition is determined not by the change of reaction kinetics (*i.e.*, intrinsic rate constants $k_1$, $k_2$, $k_{-1}$, and $k_{-2}$) as was the case in previous studies but by the relative binding between enzyme, substrate, and inhibitor. This conclusion also stipulates that one can apply traditional enzyme inhibitor formalisms to describe NP inhibition of GAL. When an inhibitor binds exclusively to the free enzyme and the conversion of substrate is prevented in such complex, the mechanism is labeled *competitive* inhibition. If the inhibitor binds only to enzyme–substrate complex, the inhibition is called *uncompetitive*. When the inhibitor could bind both to the free enzyme and intermediate complex, it is denoted as a *noncompetitive* (*mixed*) mechanism. The inhibition kinetics and mechanism for GAL by different ZnO NPs can be analyzed using the Michaelis–Menten equation, $V_o = [V_{max} \cdot S/(K_m + S)]$, where $V_o$ is initial rate of the enzyme reaction, $S$ is the concentration of substrate, $V_{max}$ is the maximum reaction rate when **E** exists primarily as complex with substrate, **ES**. $K_m$ is the Michaelis constant which gives the numerical value of the substrate concentration when reaction rate is equal to half of $V_{max}$; it describes the affinity of the enzyme for the substrate.[24] The three inhibition mechanisms can be distinguished by the difference in trends in $V_{max}$ and $K_m$ expressed as plots relating the initial rates and substrate concentration also known as Lineweaver–Burk analysis.

With the use of this conceptual framework of traditional biomolecular inhibitors to describe the inhibitory effects of NPs, nanospheres had little effect on the enzymatic activity of GAL and resulting Lineweaver–Burk plot (Figure 2E); $K_m$ of GAL in the presence of nanospheres remained unchanged at 178 $\pm$ 5.5 $\mu$M. Note that this value of $K_m$ is typical for galactosidase–RGP pair. Likewise, nanospheres had very little effect on $V_{max}$ of GAL (Figure 1E). In the case of nanoplates, $K_m$ increases as the concentration of nanoplates increased (Figure 1F), while $V_{max}$ remained unchanged (Figure 1E). For nanopyramids, one can observe consistent monotonic increase in $K_m$ with concomitant reduction of $V_{max}$ for GAL as the concentration of nanopyramids increased (Figure 1E,F). These trends of change for both $K_m$ and $V_{max}$ of GAL in the presence of ZnO nanopyramids could be also confirmed by another graphical representation of enzyme kinetics, Eadie-Hofstee plot (Supporting Information Figure S1E). The values of *y*- and *x*-intercepts, which indicate $V_{max}$ and $V_{max}/K_m$, respectively, decrease with increasing concentration of ZnO nanopyramids (Figure 1F). Therefore, the binding affinity of substrate, *i.e.* RGP to GAL, is reduced by both nanopyramids and nanoplates. However, there is no significant difference between $K_m$ values for the same concentrations of nanopyramids and nanoplates, implying that the relative effect of nanopyramids and nanoplates on the binding of RGP to GAL is similar.

Translating this data to Lineweaver–Burk analysis allowed for relative comparison of the differential effect of shape and delineated the specific inhibition mechanism. For nanoplates, the slopes in the Lineweaver–Burk plots (Figure 2C–E) increased with increasing concentration of nanoplates, while the *y*-intercepts were almost unchanged (Figure 2D). In terms of the Michaelis–Menten description of inhibition kinetics, the gradual increase in $K_m$ and relatively unchanged $V_{max}$ for nanoplates match the *competitive* inhibition mechanism; the $K_i$ for this competitive inhibition behavior was *ca.* 3 $\mu$M.

In the case of nanopyramids, both the slopes and *y*-intercepts increased with increasing concentration of NPs (Figure 2C). Such trends are not frequent among traditional inhibitors and correspond to *noncompetitive* or *mixed* inhibition behavior. That is, both the ability of

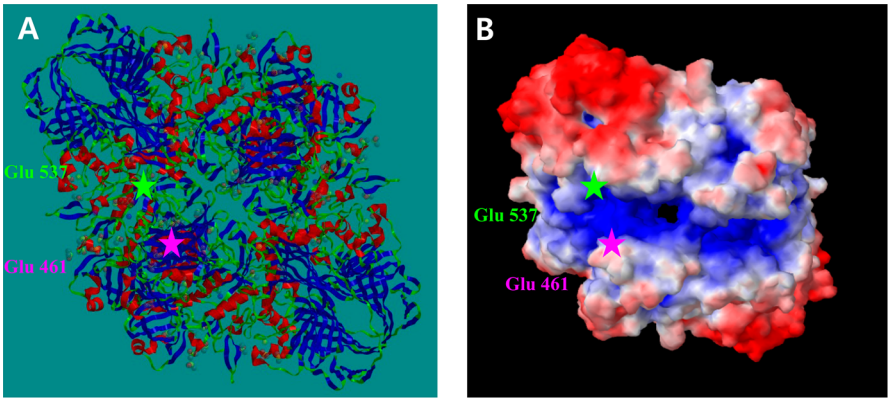


**Figure 3. Three-dimensional (A) molecular structure and (B) map of electronic potentials of GAL. Blue and red colors indicate areas with relatively positive and negative molecular potential, respectively. Approximate location of the essential amino acids of the active site is highlighted with green and magenta stars.**

the substrate to bind to the reactive center and the enzyme's ability to carry out the catalytic reaction are reduced. Combination of these effects yields a synergistic increase in the inhibitory activity. With the use of the Lineweaver–Burk data (Supporting Information Figure S4), the competitive binding constant between the enzyme and the inhibitor was calculated to be $K_i = 0.72\ \mu$M, whereas the binding constant for the inhibitor and enzyme–substrate complex (representing the uncompetitive component leading to dependence of $V_{max}$ on the inhibitor concentration) was calculated to be $\alpha K_i = 1.39\ \mu$M. One can see that the inhibitor binds more readily to the free enzyme than the enzyme–substrate complex but only by a factor of 2. Given that these NPs are not true substrate or transition state analogues in chemical structure, this is not entirely surprising. The values of $K_i$ and $\alpha K_i$ place nanopyramids among the best known natural inhibitors for GAL.[25]

Looking into greater details of the inhibitory activity, the decrease of $V_{max}$ in the presence of nanopyramids suggests that the substrate concentration has no influence on the degree of enzyme inhibition and the inhibition ability of nanopyramids is preserved even at high concentrations of RGP. That is, RGP cannot outcompete the ZnO nanopyramids, which leads to high inhibitory activity. Considering that the maximum reaction rate according to eq 1 is defined as $V_{max} = k_2 \cdot E_o$, where $E_o$ is the total concentration of enzyme and $k_2$ characterizes how fast **ES** converts into **P**,[24] the decrease of $V_{max}$ in the presence of nanopyramids should originate from the concentration decrease of $E_o$ due to the overall constant value for $k_2$ (Supporting Information Table S2). Since the measurements of enzyme activity were conducted with the same initial concentration of GAL, the decrease of $E_o$ originates from a decrease in the relative number of GAL molecules displaying catalytic activity with increasing concentrations of nanopyramids.

Since there are no denaturation-related structural changes in GAL upon interactions with NPs as indicated by UV–vis (Supporting Information Figure S3) and circular dichroism (CD) (Figure 2A) spectra,[26] a more specific shape-dependent binding between ZnO NPs and GAL attributed to noncovalent and nonelectrostatic forces (Supporting Information Table S1) is responsible for the inhibition. Indeed, electrophoretic mobility assays between GAL and the various ZnO NP shapes indicate that GAL was bound more tightly to nanopyramids than nanoplates and significantly more so than to nanospheres (Figure 2B). The trend here repeats the trend in inhibition activity in Figure 1D. Note that GAL–NP binding may not be associated with a specific stoichiometry as is the case of many traditional inhibitors. Due to the high strength of van der Waals attraction associated with the semiconductor core of the NPs and multiple hydrogen bonding sites on their surface, the association of enzyme and NPs can occur in multiple points on the protein surface. While some of these binding events could be nonspecific and shape-independent, some of them are. Finding reversible conditions for protein–NP association is essential, therefore, for observation of such phenomena.

To explain why the inhibitory activity and binding between GAL and ZnO NPs are dependent on the shape, it is instructive to correlate the kinetic data with the location of the active site on the molecular structure of the enzyme. The functional form of GAL is known to be a tetramer composed of four identical subunits (Figure 3A).[23] There is a continuous network of grooves running along the GAL surface (Figure 3B). The four active sites are located at the bottom of such surface grooves and correspond to residues 335–624 in each of the monomers forming the tetrameric barrel protein.[23] The first step in the molecular operations of the active site is believed to be the formation of a covalent bond between galactose and Glu 537 initiated by proton donation from Glu 461. The second step is the displacement of the substrate with water initiated by proton abstraction by Glu 461. The distance between Glu 537 and Glu 461 is *ca* 3.5 nm, while the molecular size of galactose is 0.6 nm. Therefore, the active site requires

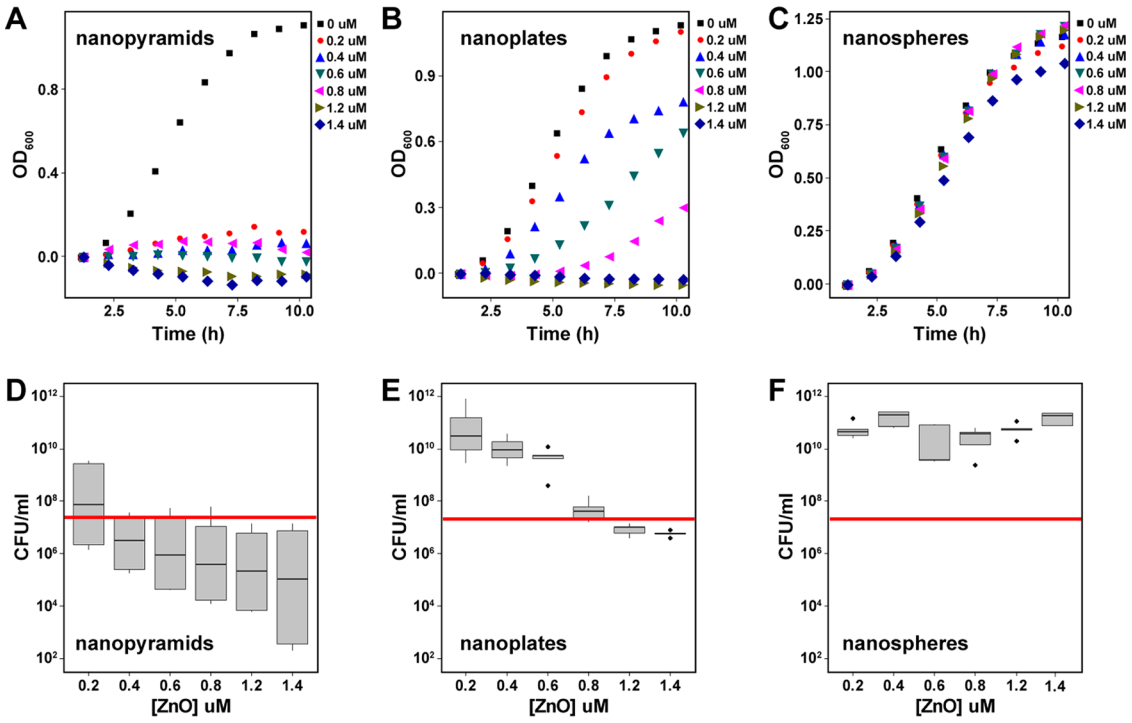


**Figure 4. (A–C) Planktonic growth curves measured turbidometrically ($OD_{600}$) for MRSA in the presence of each of the three ZnO NPs shapes at various concentrations from 0 to 1.4 $\mu$M. (D–F) Box plots of bacteria concentration after 10 h of growth expressed as colony forming units per milliliter (CFUs per mL). The limit of detection was 200 CFUs/mL. The red line represents the MRSA concentration starting inoculum at time 0.**

substantial geometrical transformation during the reaction. Although more detailed studies of the association patterns between GAL and NPs are needed, one can hypothesize that the inhibitory action of the NPs could be related to their interference with the molecular mobility of the reactive center facilitated by site-specific electrostatic attraction to the domain surrounding it (Figure 3B). The interplay of the complex electrostatic interactions determined by the potential map (Figure 3B), hydrogen bonds, vdW interactions, and the shapes of the protein and the NPs results in the strong shape dependence of the inhibitory activity of NPs. One depiction of such shape effect can be the ability of nanoplates and nanopyramids to partially penetrate into the grooves where the active center is located and interfere with its reconfiguration needed for the catalytic reaction. Other geometries of NP-GAL complexes that can give preference to reversible intermolecular binding to association with pyramidal NPs, are certainly possible, too. Regardless of particular "docking" modality, greater inhibitory activity of nanopyramids compared to nanoplates is attributed to better geometrical match with the enzyme surface due to sharper apexes and edges.[20] Enhanced inhibitory activity compared with traditional inhibitors is related to the fact that the relatively small molecules of substrate have particular difficulty in displacing the comparatively heavy NPs.

The mode of NP–enzyme interaction described above is unlikely to lead to high specificity of inhibition. Nevertheless, it can play a considerable role in biology. Moreover, their ability to interact with multiple structurally similar enzymes and enhanced resilience against biodegradation characteristic for inorganic materials can be great advantage for many applications exemplified here by the antibacterial activity of ZnO NPs. ZnO NPs are known to have a broad spectrum of antibacterial action which has often been associated with the generation of reactive oxygen species (ROS)[27,28] or disruption of bacterial cell wall (see Supporting Information). However, these hypotheses cannot explain antibacterial action of ZnO in its entirety, for instance, their high antibacterial activity in the absence of light and the increased efficacy with reduction in particle size.[29,30] Inhibition of a family of enzymes represented by GAL leading to global dysfunction of the organism could also be a mechanism of the antibacterial properties of ZnO NPs. It is also known that many enzymes responsible for ROS scavenging require divalent cofactors like GAL, and thus, the higher concentration of ROS can be a byproduct of their inhibition.

If inhibition of GAL-like enzymes contributes to the antibacterial action, one would expect a similar pattern of shape-specific inhibition of bacterial growth as was seen for GAL. Other mentioned mechanisms would likely favor the nanospheres to be most inhibitory due to small size and high surface area to weight ratio. We tested this hypothesis by examining planktonic growth of Methicillin resistant *S. aureus* (MRSA) in the presence of various concentrations of ZnO nanoplates, nanospheres, and nanopyramids. Bacterial growth

was inhibited by ZnO NPs in a shape-specific pattern identical to that for GAL inhibition (Figure 4A–C). The pyramids had near-complete inhibition at all concentrations tested. Nanoplates showed a dose-dependent inhibition and spheres showed almost no inhibition.

To confirm the role of NP geometry in antibacterial activity and avoid potential interference from the turbidity of NP dispersions, we also enumerated the actual colony forming units for a subset of the planktonic cultures in the presence of each for NP shape (Figure 4D–F). Unlike the other shapes, ZnO nanopyramids revealed not only suppressive but also bactericidal function at higher doses. This set of experiments provided additional support to the strong shape-dependence of the antibacterial function of ZnO NPs and the role that enzyme inhibition may play in it.

## CONCLUSIONS

For any concentration, ZnO nanopyramids show much greater inhibition of GAL compared with those of nanoplates and nanospheres. From the investigation of enzyme kinetics *via* Michaelis–Menten formalism, Lineweaver–Burk analysis, and Eadie-Hofstee analysis, it is found that ZnO nanoplates and nanopyramids follow *competitive* and *noncompetitive* (or *mixed*) inhibition mechanisms, respectively, while nanospheres have little effect on GAL activity. The shape-dependent inhibition behavior is associated with several factors determining the association of NPs and the enzyme with geometrical match at molecular and nano scales between the enzyme surface around the active center and ZnO nanopyramids being one of them. This inhibition mechanism is unlikely to be specific to a particular enzyme which differentiates biomimetic NP inhibitors from evolution-tuned biological inhibitors possessing lock-and-key molecular match. While being a limiting factor for some biomedical areas, this mechanism opens the possibility for the purposeful engineering of ZnO NPs as broad spectrum inhibitors, for instance, for bacterial enzymes bearing structural similarities to GAL. Discovery of synthetic methods for synthesis of chiral NPs and other nanostructures, makes possible enhancing (when necessary) the specificity of NP-enzyme association.[32,33,34]. Considering the fact that the rate of MRSA infections has risen 12-fold for the past decade and is spreading now from hospitals to community outbreaks, a broad spectrum antibacterial resilient to potential mutations of the bacteria altering molecular structure of the typical drug targets is much needed.

The findings presented here denote a shift in the conceptualization of NPs in biological systems from delivery vehicles to nanoscale biomimetic entities with distinct biological function. Looking further, one can also see a possibility of a broad spectrum of interactions between inorganic NPs and microbial ecosystems.

## EXPERIMENTAL SECTION

**Materials.** $\beta$-Galactosidase from *Escherichia coli* (GAL) and resorufin $\beta$-D-galactopyranoside were purchased from Sigma and used without further purification. Zn acetate dihydrate, $Zn(CH_3COO)_2 \cdot 2H_2O$, was purchased from Aldrich. Buffer solution (pH 7.5) and tetrabutylammonium bromide were obtained from Fluka. Sodium resorufin was obtained from Molecular Probes, Invitrogen.

**Synthesis of ZnO NPs.** We have previously described the synthesis of nanopyramids.[1] In a typical method of the preparation of nanoplates, 2.75 g of $Zn(CH_3COO)_2 \cdot 2H_2O$ in 150 mL of ethanol was heated to reflux with stirring for 1 h, and then 0.5 g of KOH dissolved in 5 mL of deionized water was added. After 12 h stirring, the white precipitates were purified by washing several times with methanol. The nanospheres were prepared by using 0.5 g of KOH dissolved in 5 mL of methanol instead of deionized water.

**Catalytic Activity Measurement of $\beta$-Galactosidase.** The concentration of GAL was kept constant at 0.4 nM while eight different concentrations of resorufin $\beta$-D-galactopyranoside within the range 20–300 $\mu$M were applied. Before the measurement of the catalytic activity, GAL was incubated with varying concentrations of ZnO NPs in 20 mM sodium phosphate buffer solution (pH 7.5) for 1 h at room temperature with gentle mixing. The catalytic reactions were started by addition of 50 $\mu$L of resorufin $\beta$-D-galactopyranoside into 100 $\mu$L of the mixture of ZnO NPs and GAL. The fluorescence intensities were observed using fluorescence microplate reader from BioTek every minute in order to determine the time profiles of product formation and the initial reaction rate ($V_0$), at each concentration of ZnO NPs. The initial linear phase lasted approximately 5 min. The intensity of fluorescence was converted into concentrations of the product (resorufin) using a fluorescence standard curve (Supporting Information Figure S1D).

**Enzyme Kinetics and Calculation of $K_i$.** The calculation of enzyme kinetics parameters followed the cannons of enzymatic catalysis represented by the reaction 1 in the main text.[2,3] Kinetic constants in this equation were calculated following the protocol as described.[4] Briefly, time-dependent profiles of **P** (Supporting Information Figure S1A–C) were found to fit very well to a two-exponential function, $I(t) = A_1 \exp(-t/\tau_1) + A_2 \exp(-t/\tau_2)$, where $\tau_1$ and $\tau_2$ are the two characteristic reaction times.[4] Using the plots of $\tau_1^{-1} + \tau_2^{-1}$ and $\tau_1^{-1}\tau_2^{-1}$ *vs* the concentrations of GAL and RGP, the four rate constants in eq 1 could be determined[3] (Supporting Information Table S2). All rate constants are specific to the enzyme–substrate pair.

The Michaelis–Menten parameters $K_m$ and $V_{max}$ for GAL with ZnO NPs, were evaluated using Lineweaver–Burk analysis, a linear transformation of the Michaelis–Menten equation and $V_o$. The nanoplates demonstrated a competitive inhibition mechanism. For this mechanism type, the $K_i$ is determined from the slope of the $K_m$ *vs* [*I*] plot as

$$\text{Slope} = \frac{K_m}{K_i} \tag{2}$$

where [*I*] in this case is the concentration of ZnO nanoplates (Figure 1F). For the mixed inhibition mechanism demonstrated by nanopyramids, we used a modified form of the classical Michaelis–Menten equation[5] and applied it to obtain the $K_i$ values for ZnO nanopyramids.

$$\frac{1}{V_m} = \frac{K_m}{V_m}\left(1 + \frac{[I]}{K_i}\right)\cdot\frac{1}{[S]} + \frac{1}{V_m}\left(1 + \frac{[I]}{\alpha K_i}\right) \tag{3}$$

To determine these parameters, we translated the specific Lineweaver–Burke plot for nanopyramids shown in Figure 2C. Specifically, we plotted the *y*-intercepts *vs* [*I*] and the slopes *vs* [*I*], where [*I*] in this case is the concentration of ZnO nanopyramids

(Supporting Information Figure S4). The *x*-intercept of the *y*-intercept *vs* [*I*] plot is equal to $-\alpha K_i$, while the *x*-intercept of the slope *vs* [*I*] plot is equal to $-K_i$. Typical values of $K_i$ for GAL inhibitors found in nature range from 2 $\mu$M to 220 mM.[6] The lowest reported value of an engineered GAL inhibitor $K_i$ is 0.11 nM.[7]

**Gel Electrophoresis.** Binding of GAL with ZnO NPs was determined using electrophoretic mobility assay using precast polyacrylamide gels. Electrophoresis runs were performed in a mini-PROTEAN Tetra cell with a constant voltage of 130 V for 1 h, and gels were placed in Coomassie stain solution. All reagents and equipment were from Bio-Rad. The patterns of the observed bands indicate that the mobility of free enzyme gradually decreases with increasing concentrations of nanopyramids. The same is observed for nanoplates, but to a lesser extent. For a given concentration of ZnO NPs, the mobilities of GAL with nanopyramids were always lower than one with nanoplates. Nanospheres had no effect on the electrophoretic mobility of the enzyme.

**Characterization.** Circular dichroism (CD) spectra were obtained using Aviv model 202 spectrometer. For each sample, five CD spectra were recorded and averaged. Then, the spectra were smoothed using Adjacent-Averaging method. UV−vis spectroscopy was carried out on an 8453 UV−vis ChemStation spectrophotometer produced by Agilent Technologies. A quartz cuvette with an optical path length of 1 cm was used for both CD and UV−vis measurements. The transmission electron microscopy (TEM) images were obtained using a JEOL 2010F analytical electron microscope at 200 keV. The zeta potentials measurements were performed by Zetasizer Nano ZS from Malvern Instruments.

**Bacterial Growth Inhibition.** Methicillin resistant *S. aureus* (MRSA) subspecies COL was used in this study. All strains were stored in glycerol at −80 °C and plated on tryptic soy agar, cultured overnight at 37 °C and stored at 4 °C. Single colony inoculates were grown in Tryptic Soy Broth + 1% glucose (w/v) (Sigma) (TSBG) under aerobic conditions for 16 h at 30 °C and diluted 1:50 in ZnO NP suspensions in TSBG to initiate planktonic growth experiments. The optical density at 600 nm was measured every hour for 10 h and normalized to the initial (time = 0) value. For quantitative cultures, 10× serial dilutions of the 10 h culture were plated and grown for 36 h at 37 °C to enumerate the number of colony forming units (CFUs) per milliliter.

*Conflict of Interest:* The authors declare no competing financial interest.

*Supporting Information Available:* The Supporting Information is available free of charge on the ACS Publications website at DOI: 10.1021/acsnano.5b03247.

Additional enzyme activity data and antibacterial effect of ZnO nanoparticles (PDF)

*Acknowledgment.* This paper is based upon work funding from NSF under Grants EFRI-BSBA 0938019; CBET 0933384; CBET 0932823, as well as from the National Research Foundation of Korea Grant funded by the Korean Government [NRF-2009-352-D00078] and [Sub No. 2013M2B2A4041436]. We are also grateful for "Research Training Grant from the Society for Academic Emergency Medicine" to Prof. J. Scott VanEpps. The authors thank the University of Michigan's EMAL for its assistance with electron microscopy, and for the NSF Grant No. DMR-9871177 for funding for the JEOL 2010F electron microscope used in this work.

## REFERENCES AND NOTES

1. Zhang, W.; Hong, D.; Zhou, Y.; Zhang, Y.; Shen, Q.; Li, J.; Hu, L.; Ki, H. Ursolic Acid and Its Derivative Inhibit Protein Tyrosine Phosphatase 1B, Enhancing Insulin Receptor Phosphorylation and Stimulating Glucose Uptake. *Biochim. Biophys. Acta, Gen. Subj.* **2006**, *1760*, 1505–1512.
2. Takahashi, T.; Mihara, H. Peptide and Protein Mimetics Inhibiting Amyloid $\beta$-Peptide Aggregation. *Acc. Chem. Res.* **2008**, *41*, 1309–1318.
3. Dorai, T.; Aggarwal, B. B. Role of Chemopreventive Agents in Cancer Therapy. *Cancer Lett.* **2004**, *215*, 129–140.
4. Halbmayr, E.; Mathiesen, G.; Nguyen, T. H.; Maischberger, T.; Peterbauer, C. K.; Eijsink, V. G. H.; Haltrich, D. High-Level Expression of Recombinant $\beta$-Galactosidases in *Lactobacillus plantarum* and *Lactobacillus sakei* Using a Aakacin P-Based Expression System. *J. Agric. Food Chem.* **2008**, *56*, 4710–4719.
5. Dodds, D. R.; Gross, R. A. Chemicals from Biomass. *Science* **2007**, *318*, 1250–1251.
6. Miranda, O. R.; Li, X.; Garcia-Gonzalez, L.; Zhu, Z. J.; Yan, B.; Bunz, U. H. F.; Rotello, V. M. Colorimetric Bacteria Sensing Using a Supramolecular Enzyme-Nanoparticle Biosensor. *J. Am. Chem. Soc.* **2011**, *133*, 9650–9653.
7. Goličnik, M.; Olguin, L. F.; Feng, G.; Baxter, N. J.; Waltho, J. P.; Williams, N. H.; Hollfelder, F. Kinetic Analysis of $\beta$-Phosphoglucomutase and Its Inhibition by Magnesium Fluoride. *J. Am. Chem. Soc.* **2009**, *131*, 1575–1588.
8. Martino, S.; Tiribuzi, R.; Tortori, A.; Conti, D.; Visigalli, I.; Lattanzi, A.; Biffi, A.; Gritti, A.; Orlacchio, A. Specific Determination of $\beta$-Galactocerebrosidase Activity *via* Competitive Inhibition of $\beta$-Galactosidase. *Clin. Chem.* **2009**, *55*, 541–548.
9. Vertegel, A. A.; Siegel, R. W.; Dordick, J. S. Silica Nanoparticle Size Influences the Structure and Enzymatic Activity of Adsorbed Lysozyme. *Langmuir* **2004**, *20*, 6800–6807.
10. Fischer, N. O.; McIntosh, C. M.; Simard, J. M.; Rotello, V. M. Inhibition of Chymotrypsin Through Surface Binding Using Nanoparticle-Based Receptors. *Proc. Natl. Acad. Sci. U. S. A.* **2002**, *99*, 5018–5023.
11. De Roe, C.; Courtoy, P. J.; Baudhuin, P. A Model of Protein-Colloidal Gold Interactions. *J. Histochem. Cytochem.* **1987**, *35*, 1191–1198.
12. Chalkias, N. G.; Kahawong, P.; Giannelis, E. P. Activity Increase of Horseradish Peroxidase in the Presence of Magnetic Particles. *J. Am. Chem. Soc.* **2008**, *130*, 2910–2911.
13. Shang, W.; Nuffer, J. H.; Muñiz-Papandrea, V. A.; Colón, W.; Siegel, R. W.; Dordick, J. D. Cytochrome *c* on Silica Nanoparticles: Influence of Nanoparticle Size on Protein Structure, Stability, and Activity. *Small* **2009**, *5*, 470–476.
14. Wang, J.; Jensen, U. B.; Jensen, G. V.; Shipovskov, S.; Balakrishnan, V. S.; Otzen, D.; Pedersen, J. S.; Besenbacher, F.; Sutherland, D. S. Soft Interactions at Nanoparticles Alter Protein Function and Conformation in a Size Dependent Manner. *Nano Lett.* **2011**, *11*, 4985–4991.
15. Pandey, P.; Singh, S. P.; Arya, S. K.; Gupta, V.; Datta, M.; Singh, S.; Malhotra, B. D. Application of Thiolated Gold Nanoparticles for the Enhancement of Glucose Oxidase Activity. *Langmuir* **2007**, *23*, 3333–3337.
16. Kotov, N. A. Inorganic Nanoparticles as Protein Mimics. *Science* **2010**, *330*, 188–189.
17. Fischer, N. O.; Verma, A.; Goodman, C. M.; Simard, J. M.; Rotello, V. M. Reversible "Irreversible" Inhibition of Chymotrypsin Using Nanoparticle Receptors. *J. Am. Chem. Soc.* **2003**, *125*, 13387–13391.
18. Jacobson, R. H.; Zhang, X.-J.; DuBose, R. F.; Matthews, B. W. Three-Dimensional Structure of $\beta$-Galactosidase from *E. coli*. *Nature* **1994**, *369*, 761–766.
19. Verma, A.; Simard, J. M.; Worrall, J. W. E.; Rotello, V. M. Tunable Reactivation of Nanoparticle-Inhibited $\beta$-Galactosidase by Glutathione at Intracellular Concentrations. *J. Am. Chem. Soc.* **2004**, *126*, 13987–13991.
20. Yang, M.; Sun, K.; Kotov, N. A. Formation and Assembly-Disassembly Processes of ZnO Hexagonal Pyramids Driven by Dipolar and Excluded Volume Interactions. *J. Am. Chem. Soc.* **2010**, *132*, 1860–1872.
21. You, C. C.; De, M.; Han, G.; Rotello, V. M. Tunable Inhibition and Denaturation of α-Chymotrypsin with Amino Acid-Functionalized Gold Nanoparticles. *J. Am. Chem. Soc.* **2005**, *127*, 12873–12881.
22. Chakraborti, S.; Chatterjee, T.; Joshi, P.; Poddar, A.; Bhattacharyya, B.; Sing, S. P.; Gupta, V.; Chakrabari, P. Structure and Acitivty of Lysozyme on Binding to ZnO Nanoparticles. *Langmuir* **2010**, *26*, 3506–3513.

23. Matthews, B. W. The Structure of *E. coli* $\beta$-Galactosidase. *C. R. Biol.* **2005**, *328*, 549–556.
24. Liu, Y.; Schanze, K. S. Conjugated Polyelectrolyte-Based Real-Time Fluorescence Assay for Alkaline Phosphatase with Pyrophosphate as Substrate. *Anal. Chem.* **2008**, *80*, 8605–8612.
25. Panday, N.; Canac, Y.; Vasella, A. Very Strong Inhibition of Glucosidases by C(2)-Substituted Tetrahydroimidazopyridines. *Helv. Chim. Acta* **2000**, *83*, 58–79.
26. Guo, S.; Zhou, Q.; Lu, T.; Ding, X.; Huang, X. Inhibition Mechanism of $Tb^{III}$ on Horseradish Peroxidase Activity. *Chem. Biodiversity* **2008**, *5*, 2050–2059.
27. Xia, T.; Kovochich, M.; Liong, M.; Mädler, L.; Gilbert, B.; Shi, H.; Teh, J. I.; Zink, J. I.; Nel, A. E. Comparison of the Mechanism of Toxicity of Zinc Oxide and Cerium Oxide Nanoparticles Based on Dissolution and Oxidative Stress Properties. *ACS Nano* **2008**, *2*, 2121–2134.
28. Lipovsky, A.; Tzitrinovich, Z.; Friedmann, H.; Applerot, G.; Gedanken, A.; Lubart, R. EPR Study of Visible Light-Induced ROS Generation by Nanoparticles of ZnO. *J. Phys. Chem. C* **2009**, *113*, 15997–16001.
29. Zhang, L.; Jiang, Y.; Ding, Y.; Povey, M.; York, D. Investigation into the Antibacterial Behaviour of Suspensions of ZnO Nanoparticles (ZnO nanofluids). *J. Nanopart. Res.* **2007**, *9*, 479–489.
30. Raghupathi, K. R.; Koodali, R. T.; Manna, A. C. Size-Dependent Bacterial Growth Inhibition and Mechanism of Antibacterial Activity of Zinc Oxide Nanoparticles. *Langmuir* **2011**, *27*, 4020–4028.
31. Bahng, J. H.; Yeom, B.; Wang, Y.; Tung, S. O.; Kotov, N. A. Anomalous Dispersions of Hedgehog Particles. *Nature* **2015**, *517*, 596–599.
32. Yeom, J.; Yeom, B.; Chan, H.; Smith, K. W.; Dominguez-Medina, S.; Hwan Bahng, J.; Zhao, G.; Chang, W. S.; Chang, S. J.; Chuvilin, A.; Melnikau, D.; Rogach, A. L.; Zhang, P.; Link, S.; Král, P.; Kotov, N. A. Chiral Templating of Self-Assembling Nanostructures by Circularly Polarized Light. *Nature Mater.* **2015**, *14*, 66–72.
33. Dolamic, I.; Varnholt, B.; Bürgi, T. Chirality transfer from gold nanocluster to adsorbate evidenced by vibrational circular dichroism. *Nat. Commun.* **2015**, *6*, 7117.
34. Chen, W.; Bian, A.; Agarwal, A.; Liu, L.; Shen, H.; Wang, L.; Xu, C.; Kotov, N.A. Nanoparticle Superstructures Made by Polymerase Chain Reaction: Collective Interactions of Nanoparticles and a New Principle for Chiral Materials. *Nano Lett.* **2009**, *9*(5), 2153–2159.